

Modelling and Experimental Verification of Heat Dissipation Mechanisms in an SU-8 Electrothermal Microgripper

Belen Solano^{a,b}, James Merrell^a, Andrew Gallant^a, David Wood^{a,*}

^aSchool of Engineering and Computing Sciences, South Road, Durham, UK, DH1 3LE

^bCentro Universitario de la Defensa, Zaragoza, 50090, Spain

*Corresponding Author Tel: +44 (0)191 3342464 e-mail: david.wood@durham.ac.uk

Keywords: Microgripper, heat dissipation, thermal imaging, electrothermal, SU-8

Abstract

Within this work, a microgripper based on a hot-cold arm principle was tested to give a greater understanding of the associated heat dissipation methods. Experiments were conducted in air at atmospheric and sub-atmospheric pressure, and in helium, argon and helium at sub-atmospheric pressure. The change in deflection, when using gases with different thermal conductivities and at varying pressures showed the significance of conduction through the atmosphere. The experimental results were found to verify a theoretical model created previously by this group, and a further model developed independently; both predicted the deflection that a given current would cause.

Introduction

The microgripper device consists of two thermal actuators that deform when a difference in temperature is induced between its arms. The microgripper is based on a U-shaped thermal actuator, which has been studied extensively in its embedded actuation version [1], i.e. where the same material, usually polysilicon, is used to produce the heating and the desired expansion. Our microgripper is made from two layers of SU-8 polymer, with embedded chromium/gold tracks to provide the electrothermal heating, and has been described previously (Figure 1, detailed in [2]). The device operation is controlled by applying a current through the conducting layer, where the dissipated power heats the surrounding material and the structure deflects in-plane due to the differential thermal expansion of its constituent parts.

The intended application is in the manipulation of cells and other small particles. Advances in biological and biomedical areas such as cloning, stem cell research or in-vitro fertilisation have demonstrated the need for complex micro-manipulation tools [3]. However, not only do such micro-manipulators have to work within the liquid environment that supports the biological cells, they have to operate at low temperatures (<50 °C) and with controllable handling forces (<40 µN), so as to not to cause any damage. As noted in earlier work [2], our design places the actuation electrodes on one arm only. In operation, this arrangement creates a maximum temperature difference between the two arms. It then allows for the maximum deflection opening of the microgripper tips for the minimum drive current and overall device temperature. By placing the heaters on the inner part of the structure, operation allows the microgripper tips to open (normally closed); conversely, placement of the heaters on the outer part of the microgripper allows the tips to close (normally open). The design then places our device in an operating parameter space (low voltage and temperature) that has eluded other devices, making this microgripper a highly flexible tool suitable for a range of biological applications. We have demonstrated how the device can provide easy manipulation of cells without any associated damage [4].

Work in [4] also showed drive current vs deflection results when the microgripper is operated in the different environments of water and air. In applications, cell manipulation would be done in a liquid ambient, whereas particle manipulations (e.g. dust or pollen in forensic applications) would be carried out in air. As expected, the significantly higher values of both viscosity and thermal conductivity associated with water produced a much smaller deflection (by a factor of ~12) than when the microgripper was operated in air under the same drive conditions.

Besides electrothermal actuation, there are alternative drive mechanisms for microgrippers, such as electrostatic [5], piezoelectric [6], electromagnetic [7], shape memory alloy [8] and those based on electroactive polymers [9]. However, it is the electrothermal microgripper that has proven to be the most enduring and extensively studied, and the heat loss mechanisms in this type of device form the basis of the current paper.

I. Device Fabrication

A fabrication route has been developed to produce a high yield of operational devices [10]. The fabrication starts with a substrate of oxidised silicon wafers, on which the first layer of SU-8, embedded chromium/gold heaters and second, thicker layer of SU-8 are deposited and patterned by photolithography. Final release of the structure is obtained by vapour phase etching in a XeF₂ environment, which removes the substrate from underneath each microgripper while

leaving the electrical contact pads intact. Device separation is achieved by breaking the silicon wafer along the crystal cleavage planes. The size of the tip opening can be made as small as 10 μm [11], the tip end shape can be modified to suit the application [10] and extra functionality can be placed on the structure, e.g. electrodes to aid in electrochemical analysis [12].

II. Modelling

We have previously developed a model which considers the interaction of electrothermal and thermomechanical effects [13]. All three heat dissipation mechanisms, as well as heat input, were introduced to give a complete analysis of the thermal behaviour and the associated steady state temperature distribution. For the volume element shown in Figure 2, the balance between the heat generated within the device and that lost by conduction through the solid beams to the anchors and to the environment can be expressed as

$$q_{gen} = q_{COND} + q_{cond} + q_{conv} + q_{rad} \quad (1)$$

where q_{gen} is the heat generated within the volume element, q_{COND} is the heat conducted through the volume element, and q_{cond} , q_{conv} , q_{rad} are respectively the heat lost into the ambient by conduction, convection, and radiation. We showed that the relevance of each mechanism can differ considerably depending on multiple factors such as the configuration of the actuator and the surrounding media.

The complete model can be described briefly as follows. First a set of semi-empirical formulae were developed for the calculation of the heat transfer coefficients to the surrounding ambient by conduction. Departing from existing 2D conduction shape factors [14], a set of new formulae were used to calculate the heat losses by conduction from a single rectangular beam, and from two closely spaced beams that lose heat conjointly. In the latter case, different formulas were used depending on the relative size of some characteristic dimensions of the system: thickness and width of the beams, and the spacing between them. All of the coefficients were validated by FEA (in this case Coventor). A single beam 1D electrothermal model was then developed that took into account the overhanging configuration of the beam, and the heat losses into the ambient by conduction as opposed to convection. This was used to obtain the temperature distribution along the extended beam (jaw) of the microgripper. The work was then extended to complete a coupled beam 1D electrothermal model that took into account the overhanging configuration of the system, the heat losses into the ambient by conduction as opposed to convection, and the heat exchange between closely spaced beams. This was used to model the behaviour of the actuators which compose the microgripper. The modelling technique included, in an iterative manner, the dependency of the SU-8 material properties, the metallisation resistivity and thermal conductivity of the air, with temperature. Finally, a 1D thermomechanical model was developed that predicted the deflection of the actuator for a given temperature difference between the arms. The model predictions were validated with a combination of temperature measurements from infrared camera images, I-V characteristics and gripper beam deflection measurements.

It was concluded in [13] that the main heat dissipation mechanism was conduction, both into the ambient atmosphere and in the gap between the adjacent parallel beams. This is because the relative effect of convection, or mass transport effects, is characterised by the Rayleigh number R_a , which is dependent on the dimensions characteristic of the system. For the dimensions, temperatures and ambient environments associated with a microgripper, R_a will have values in the 10^{-3} to 10^{-1} range, whereas for a more typical macroscopic problem R_a will be $\sim 10^{10}$. The model developed in [13] was verified by experimental data to show that the contribution of mass transport (i.e. convection) is negligible compared to pure thermal conduction within a stationary mass of air or water. Similarly, for the dimensions and temperatures involved, the contribution of radiation to the overall heat loss is also very small. Work presented in this current paper was undertaken to further validate the effect of conduction into the ambient; with a combination of reduced pressure and/or different thermal conductivity ambients, the importance of this heat loss mechanism was expected to become apparent.

Modelling work reported previously [15] for a thermal actuator of a very different design has shown a reduced drive current in a vacuum ambient can give the same deflection as the current needed in air (ratio $\sim 1:3.6$), although this was not verified experimentally.

Results and Discussion

A microgripper was operated from a constant current supply (up to 80 mA) in a windowed, enclosed environmental chamber. Experiments to validate the model were conducted in air, helium and argon ambients and in air and helium at sub-atmospheric pressures. The change in deflection with drive current was observed with a microscope and associated viewing software, with an image resolution of 0.3 pixels per micron. Deflection vs current data when using gases with different thermal conductivities (Figure 3), at varying pressures (Figure 4) and with changes in both thermal conductivity and pressure (Figures 5 and 6) showed the significance of conduction through the atmosphere.

I. Different Thermal Conductivity Ambient

Both helium and argon were used as ambient gases in place of air; these gases have thermal conductivities k of 0.142 W/mK and 0.016 W/mK respectively (for air, $k = 0.024$ W/mK – [16], all values at 25 °C). It can be seen that the high thermal conductivity of helium leads to a greater drive current being needed to obtain a given deflection than in air (Figure 3), and similarly the drive current in argon is reduced compared to that in air. For a given deflection, e.g. 60 μm , the ratio of drive currents helium:air (1.95:1) is much larger than the equivalent value for air:argon (1.14:1), consistent with the relative differences in thermal conductivity between the gases.

II. Reduced Pressure Air Ambient

An air ambient was then used and the pressure reduced gradually to 16 Pa. It was found that, as the pressure reduced, the net deflection for a given current increased (Figure 4). The decrease in the number of molecules and the increase in the size of their mean free path (MFP) - below ~ 130 Pa, the MFP is of a similar magnitude to the gap between the gripper arms - meant that limited conduction could take place. The net deflection of the device therefore increased. Below 16 Pa, the deflection changes were not considered significant and these results are not presented here.

The mean free path of an air molecule at a pressure of 1200 Pa is 3.8 μm , whereas at 16 Pa the MFP is 283 μm . The gap between the hot and cold arms of an actuator is 60 μm , and the length of the actuator arm is 2000 μm . This is important because it shows that at low pressures the MFP is much larger than the gap between the arms. Conduction relies upon the interaction of the air molecules between each other and the gripper surfaces. Consequently such a large MFP in relation to the gripper geometry severely limits the amount of heat transfer from the device. This explains why at low pressures the net deflection was greater. Whereas at higher pressures (e.g. in the region of 1200 Pa) where the MFP is smaller, there was a greater chance of the air molecules making contact with the gripper and each other. Subsequently a greater amount of conduction took place and the deflection was less.

For a typical deflection of 60 μm , the current needed in air (30.7 mA) was ~ 2.8 times higher than that needed at a pressure of 16 Pa (10.9 mA). This ratio is consistent with the modeling only ratio of 3.6:1 presented in [8] for a different thermal actuator. The exact number associated with this current ratio will depend on device design; materials, dimensions and surface area:volume ratio will all have a significant role to play.

III. Different Conductivity and Pressure Ambient

As the value of thermal conductivity of a gas decreases with pressure, it might be expected that the deflection values for different ambients at sub-atmospheric pressure would be very similar. This was confirmed when the pressure of helium was reduced, as shown in Figure 5 for five separate low pressure readings. However it can be seen that as the pressure is increased the net deflection in helium is consistently slightly less than in air - Figure 6 shows this phenomenon in more detail at a pressure of 1200 Pa.

In addition the mean free path of the gas was found to be a significant factor. Using equation 2 the MFP of a gas can be calculated; where L is the mean free path (m), η is the viscosity (Poise), P is the pressure (Pa), T is the temperature (Kelvin) and M is the molecular mass of the gas (g/mol).

$$L = 11.46 \eta / P (T/M)^{1/2} \quad (2)$$

For helium, the MFP is 291.9 μm and 9.7 μm at a pressure of 40 Pa and 1200 Pa respectively. The MFP for air is 113.3 μm at 40 Pa and 3.8 μm at 1200 Pa. The MFP at 40 Pa for both air and helium is so large in comparison to the distance between the hot and cold arms of the actuator (60 μm) that little conduction through the air can take place. Consequently any difference in the thermal conductivity of the gas has little effect. At higher pressures, e.g. 1200 Pa where the MFP is 3.8 μm in air, the higher thermal conductivity of the gas has a greater influence on the amount of heat dissipated from the device. This reinforces the fact that at higher pressures (where the MFP is smaller), conduction through the air plays a significant part in transferring heat from the device.

Conclusion

From deflection vs drive current experiments in air, helium and argon it has been found that the thermal conductivity of the gas has a significant influence on the deflection of the device.

It has been found that as the pressure of the ambient air is reduced the deflection increases for a given current, down to a pressure value of 16 Pa. At lower pressures there are fewer air molecules present to transfer the heat from the device via conduction, and below 16 Pa the deflection changes were insignificant. As the pressure approaches this value the MFP of an air molecule becomes comparable to and then surpasses the dimensions of the device, and

conduction is less effective at transferring heat away from the device. This results in a higher temperature within the gripper arms and a greater deflection. For a given deflection, the ratio between the current needed at atmospheric:reduced pressure is 2.8:1, in good agreement with modeling predictions.

It has been found that when a gas other than air is taken to sub-atmospheric pressures there is little difference in the net deflection of the microgripper. As thermal conductivity of a gas decreases with pressure, an increase in the size of the mean free path means less conduction takes place through the atmosphere.

All the above experiments confirm that conduction through the atmosphere is the significant method of heat transfer from the device.

References

- [1] N Chromis and L Lee, *IEEE Journal of Microelectromechanical Systems* 14, pp 1-7, 2005.
- [2] B Solano and D Wood, *Microelectronic Engineering* 84, pp 1219-1222, 2007.
- [3] C Yi, C Li, S Ji and M Yang, *Analytica Chimica Acta* vol 560, pp 1-23, 1996.
- [4] B Solano, A J Gallant and D Wood, *Proc 10th Symposium on Design, Test, Integration and Packaging of MEMS and MOEMS*, Rome, Italy, 1-3 April, 2009, pp 61-65.
- [5] F Beyeler, A Neild, S Oberti, D J Bell, Y Sun, J Dual and B J Nelson, *IEEE Journal of Microelectromechanical Systems* 16, pp. 7-15, 2007.
- [6] S K Jericho, M H Jericho, T Hubbard and M Kujath, *Review of Scientific Instruments* 75, pp. 1280-1282, 2004.
- [7] D H Kim, M G Lee, B Kim and Y Sun, *Smart Materials & Structures* 14, pp. 1265-1272, 2005.
- [8] M Kohl, B Krevet and E Just, *Sensors and Actuators A* 97-8, pp. 646-652, 2002.
- [9] E W H Jager, O Inganas and I Lundstrom, *Science* 288, pp. 2335-2338, 2000.
- [10] R Daunton, A J Gallant and D Wood, *Proc Materials Research Society Meeting*, San Francisco, USA, 9-13 April, 2012, vol 1463, paper mrss12-1463-qq02-10.
- [11] R Daunton, A J Gallant and D Wood, *IOP J Micromechanics and Microengineering* 22, 075016, 2012.
- [12] R Daunton, A J Gallant, R Katakya and D Wood, *Chemical Communications* 47, pp 6446-6448, 2011.
- [13] B Solano, S Rolt and D Wood, *Proc. Inst. Mech. Engrs. part C* 222, pp 73-86, 2008.
- [14] F Incropera and D DeWitt, *Fundamentals of Heat and Mass Transfer*, 4th ed. New York: Wiley, 1996.
- [15] C Lott, T McLain, J Harb and L Howell, *Sensors and Actuators A* 101, pp 239-250, 2002.
- [16] http://www.engineeringtoolbox.com/thermal-conductivity-d_429.html

Figure Captions

Figure 1. Detail of the fabricated device and the tips of the jaws.

Figure 2. Heat dissipation routes of a volume element of the hot arm.

Figure 3. Gripper deflection behaviour as a function of ambient gas composition.

Figure 4. Gripper deflection behaviour as a function of ambient air pressure. Pressure values are indicated in Pa.

Figure 5. The net deflection compared in helium and air at lower than atmospheric pressures. Pressure values are indicated in Pa.

Figure 6. More detail on the comparison between helium and air at 1200 Pa pressure.

Figure 1

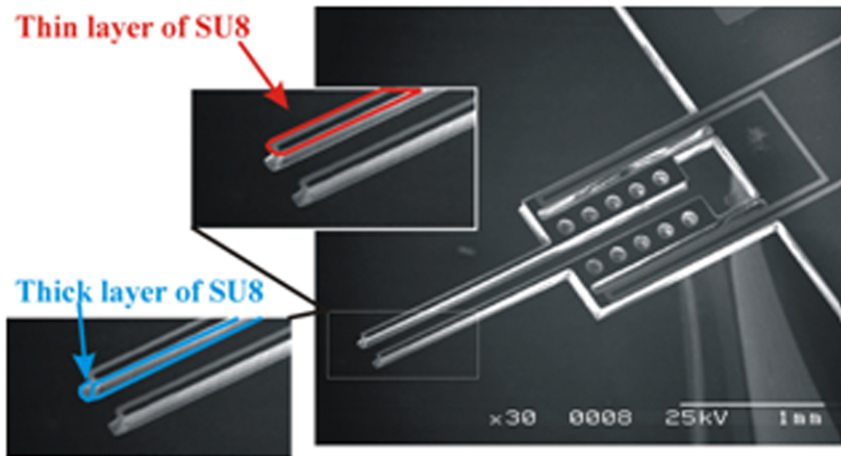


Figure 2

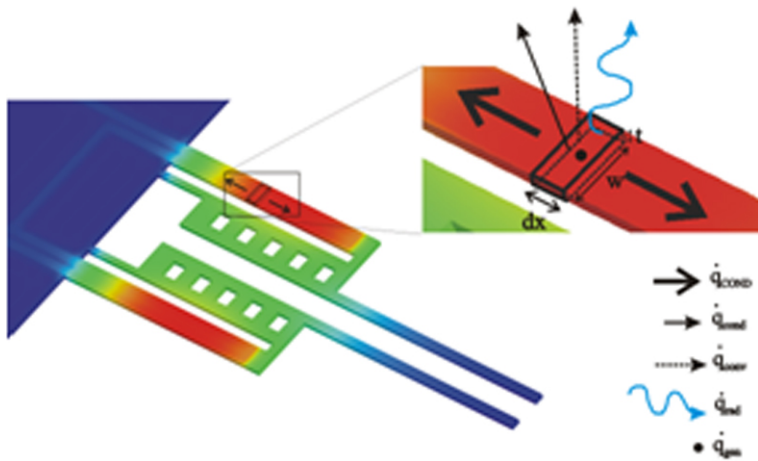


Figure 3

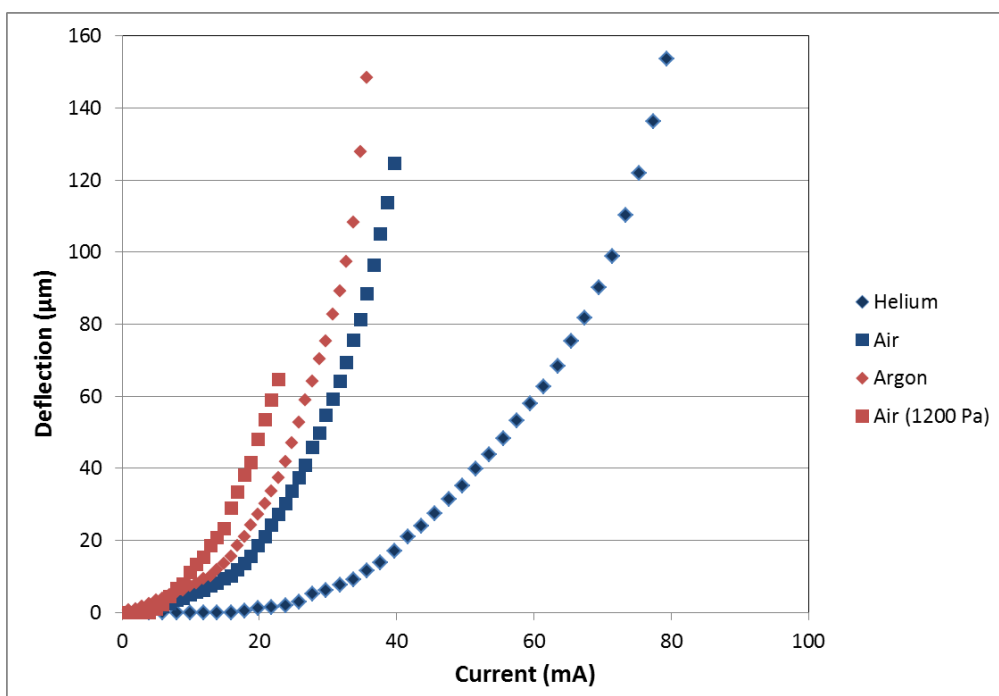


Figure 4

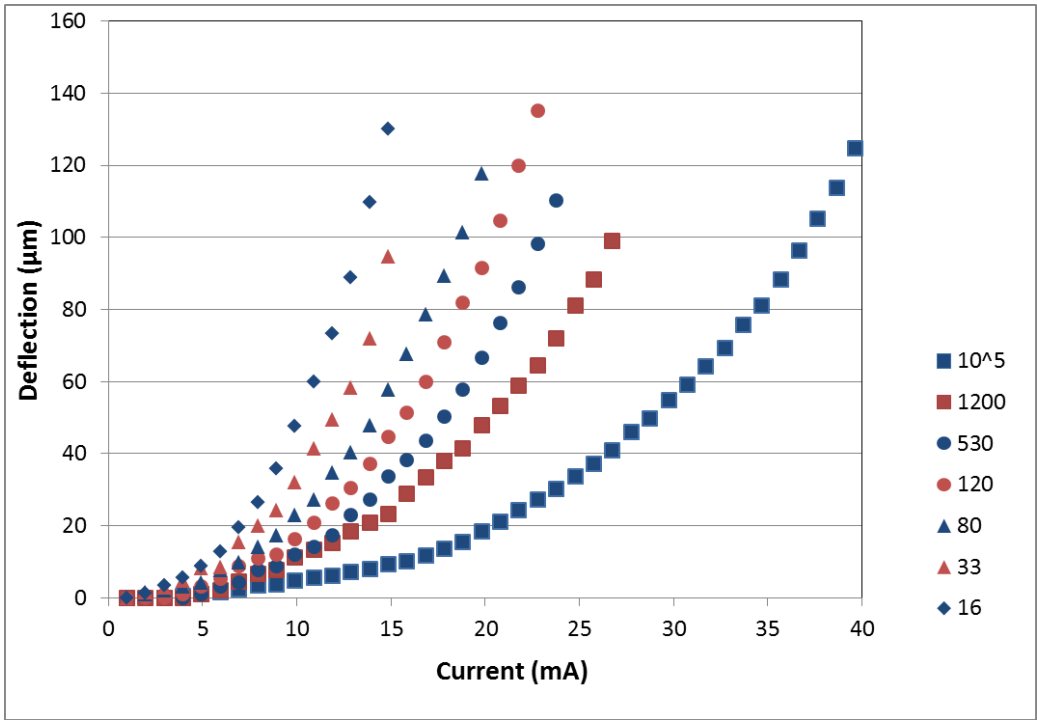


Figure 5

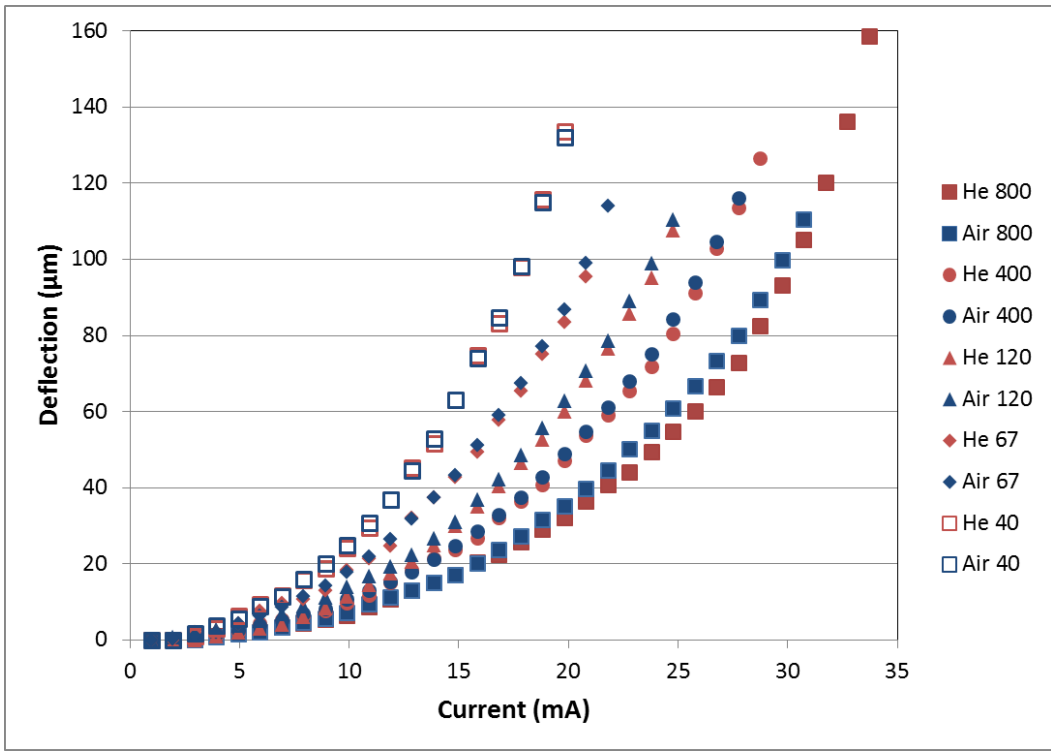


Figure 6

